ChemPubSoc Europe

DOI: 10.1002/cctc.201402573

# Selective Hydrogenation of Cinnamaldehyde to Cinnamal Alcohol over Platinum/Graphene Catalysts

Xiwang Ji,[a] Xiaoyu Niu,[a] Bo Li,*[c] Qing Han,[a] Fulong Yuan,[a] Francisco Zaera,*[b] Yujun Zhu,*[a] and Honggang Fu[a]

Catalysts made of Pt nanoparticles dispersed on graphene (*X* wt%Pt/G, *X* = 2.0, 3.5, and 5.0) were prepared and characterized by XRD, Raman spectroscopy, BET surface area measurements, TEM, and X-ray photoelectron spectroscopy (XPS), and a 3.5 wt% Pt supported on Vulcan Carbon catalyst (3.5 wt%Pt/VC) was included as a reference. Although the mean Pt nanoparticle size is approximately 4.4 nm for all *X* wt%Pt/G and 3.5 wt%Pt/VC catalysts, cinnamal alcohol was produced with high selectivity only with the graphene-supported catalysts: 92% conversion and 88% selectivity toward cinnamal alcohol were obtained with 3.5 wt%Pt/G. This catalyst also showed good stability in recycling tests. The good selectivity observed with the graphene-based catalysts is attributed to the higher fraction of reduced surface $Pt^0$ atoms seen on the surface of the Pt nanoparticles (determined by XPS). This interpretation is consistent with DFT calculations. Additional π–π interactions between cinnamaldehyde and graphene may also play a role in the selective hydrogenation of cinnamaldehyde.

## Introduction

The selective hydrogenation of α,β-unsaturated carbonyl compounds is of theoretical and practical significance.[1–3] For instance, the hydrogenation of cinnamaldehyde (CAL) can produce cinnamal alcohol (COL), hydrocinnamaldehyde (HALD), and/or hydrocinnamal alcohol (HALC; Scheme 1), but the selective production of COL is difficult because the hydrogenation of the C=C bond is thermodynamically favored over that of the C=O moiety.[1,4] Moreover, acetals and other unidentified high-molecular-weight compounds can also be produced in large quantities in these reactions.[4,5] Although much research has already been focused on this issue, the selective hydrogenation of α,β-unsaturated aldehydes remains a challenge.

The selective hydrogenation of α,β-unsaturated aldehydes toward the unsaturated alcohol can be achieved with homogeneous catalysts such as metal hydrides, aluminium isopropoxide, and others.[6,7] However, it is desirable to develop an equally selective heterogeneous catalyst as these are easier to handle and separate from the products. To this end, a large number of studies on supported catalysts based on Pt, Rh, Au, Ru, and Pd active phases have been reported.[8–12] Cordier et al. reported that the selectivity for COL production from CAL hydrogenation follows the sequence Os > Ir > Pt > Ru > Rh > Pd,[13,14] a trend that was correlated with the width of the d-band of the metal (Pd < Pt < Ir, Os). Many other studies have targeted supported Pt catalysts because of their high activity and moderate selectivity.

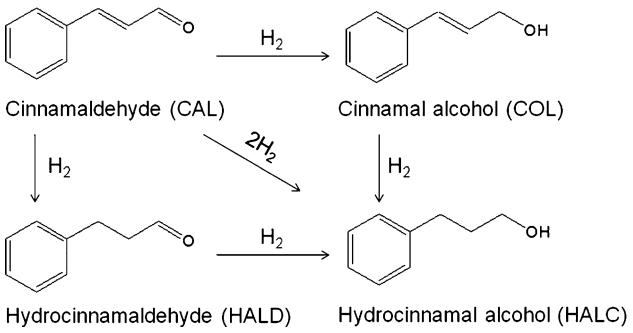


**Scheme 1.** Hydrogenation of CAL.

In addition to the different metals that can be used to control selectivity in CAL hydrogenation processes, the supports may play an important role to define the selectivity. Indeed, differences in activity and selectivity may be obtained by varying the nature of the interaction between the support and nanoparticles (NPs). For instance, the selectivity toward COL production may be enhanced by using reducible oxides such as $CeO_2$,[15] $MnO_2$,[16] $SnO_2$,[17] $TiO_2$,[18] and ZnO[19] because of the electron transfer that takes place between these supports and

[a] X. Ji, Dr. X. Niu, Q. Han, Prof. F. Yuan, Prof. Y. Zhu, H. Fu
Key Laboratory of Functional Inorganic Material Chemistry
(Heilongjiang University), Ministry of Education
School of Chemistry and Materials
Heilongjiang University
72 Xuefu Road, Harbin 150080 (China)
E-mail: yujunzhu@hlju.edu.cn

[b] Prof. F. Zaera
Department of Chemistry
University of California, Riverside
900 University Avenue, Riverside, California 92521 (United States)
E-mail: zaera@ucr.edu

[c] Dr. B. Li
Shenyang National Laboratory for Materials Science
Institute of Metal Research, Chinese Academy of Sciences
72 Wenhua Road, Shenyang 110016 (China)
E-mail: boli@imr.ac.cn

Supporting information for this article is available on the WWW under http://dx.doi.org/10.1002/cctc.201402573.

  

the metallic phase. Moreover, weak Lewis sites on the support, especially in the vicinity of the Pt NPs, may aid in the adsorption of CAL and HALD through an interaction of their polar carbonyl function (C=O).[20,21] This adsorption mode could assist in the preferential formation of alcohols.

In recent years, thanks to their unique structures and properties, advanced carbon materials such as carbon nanofibers (CNF), carbon nanotubes (CNT), and graphene have attracted a great deal of attention as possible materials for metal-free heterogeneous catalysts,[22,23] electrochemical energy storage devices,[24] and fuel cells.[25,26] In particular, graphene, a two-dimensional planar carbon material first obtained from graphite in 2004, is regarded as a promising electrocatalytic material.[27,28] Graphene can interact strongly with both transition metals and aromatic compounds: theoretical calculations and experimental results have indicated that some electron transfer may occur between the supported Pt NPs and the graphene support,[29,30] and thanks to the large π system of graphene, guest molecules with π orbitals can be adsorbed readily on its surface by π–π interactions.[31,32] In one case, Li et al.[33] explained the excellent catalytic performance seen for the catalytic reduction of 4-nitrophenol (4-NP) with a Au/graphene hydrogel solid by the high adsorption ability of graphene towards 4-NP and a synergistic effect between the graphene and the Au NPs.

In the hydrogenation of CAL, it could be envisioned that the aromatic ring may interact through its π electrons with the basal plane of graphene to facilitate a flat adsorption geometry,[34] which provides a unique geometrical arrangement for the potential selective hydrogenation of the carbonyl group by adjacent Pt NPs. Indeed, previous publications of CAL hydrogenation on reduced graphene oxide catalysts have reported a good selective performance.[35] However, the effect of the Pt species and the interaction between Pt and reduced graphene oxide on the catalytic activity were not discussed in detail.[35] To test this hypothesis, a number of Pt/graphene catalysts were prepared and used for the selective hydrogenation of CAL. The catalytic performance of the graphene support was contrasted with that of other more conventional carbon-containing solids, and the effect of Pt loading was evaluated in terms of catalytic activity and selectivity and interpreted with the help of theoretical calculations.

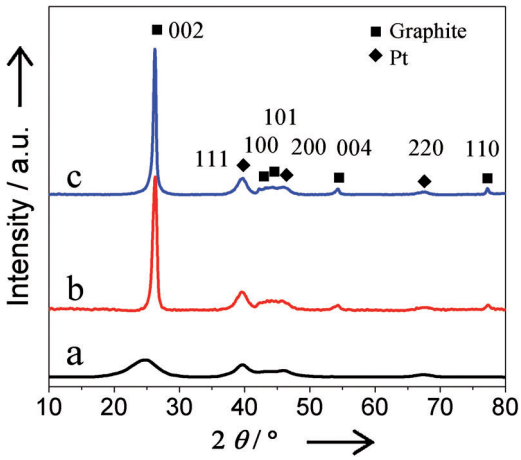


**Figure 1.** XRD patterns of a) 3.5 wt%Pt/VC, b) 3.5 wt%Pt/G, and c) 3.5 wt%Pt/G-r (recycled).

and 77.4° (110) correspond to the 2D in-plane symmetry along the graphene sheets.[36] Although some broad features caused by carbon are seen in the XRD pattern of 3.5 wt%Pt/VC, it is clear that the as-prepared graphene support has a better crystallinity than the VC support. Additional diffraction peaks were seen in the patterns of both catalysts at around $2\theta = 39.7$, 46.4, and 67.5°, which correspond to the (111), (200), and (220) crystalline planes of the face-centered cubic (fcc) Pt particles, respectively.[26] The average diameters of the Pt NPs (calculated by using the full width at half maximum of the Pt(111) reflection and Scherrer's equation[37]) are approximately 3.8 and 4.3 nm for 3.5 wt%Pt/VC and 3.5 wt%Pt/G, respectively (Table 1).

**Table 1.** Characterization of 3.5 wt%Pt/G and 3.5 wt%Pt/VC.

| Catalyst | $S_{BET}$ [$m^2 g^{-1}$][a] | Pt size [nm][b] | Pt size [nm][c] | $I_D/I_G$[d] | Content of Pt species [%]/BE [eV][e] | | |
|---|---|---|---|---|---|---|---|
| | | | | | $Pt^0$ | $Pt^{II}$ | $Pt^{IV}$ |
| 3.5 wt%Pt/G | 57 | 4.4 | 4.3 | 0.29 | 61/71.4 | 29/72.6 | 10/74.9 |
| 3.5 wt%Pt/VC | 198 | 3.9 | 3.8 | 1.2 | 42/71.6 | 26/72.8 | 32/74.8 |
| 3.5 wt%Pt/G-r[f] | 56 | 4.4 | 4.4 | 0.32 | 59/71.4 | 29/72.4 | 12/74.9 |

[a] BET surface area. [b] Calculated from TEM images. [c] Calculated from the Pt(111) XRD peak and Scherrer's equation. [d] From Raman spectra. [e] Calculated from Pt4f XPS spectra. [f] 3.5 wt%Pt/G after four consecutive catalytic runs.

## Results

### Catalyst characterization

Catalysts made of Pt NPs dispersed on graphene (*X* wt%Pt/G, $X = 2.0$, 3.5, and 5.0) were prepared, and a 3.5 wt% Pt supported on Vulcan Carbon catalyst (3.5 wt%Pt/VC) was synthesized as a reference. The XRD patterns obtained for 3.5 wt%Pt/G and 3.5 wt%Pt/VC are shown in Figure 1. The diffraction peaks seen at $2\theta = 26.4$ (002) and 54.6° (004) in the pattern of the graphene-based sample are characteristic of the parallel graphene layers, whereas the diffraction peaks at $2\theta = 42.5$ (100)

Raman spectroscopy was used to investigate the degree of crystallinity of the carbon supports (Figure 2). The two prominent peaks seen in the Raman spectra shown in Figure 2, the D ($\tilde{\nu} = 1353\ cm^{-1}$) and G ($\tilde{\nu} = 1560\ cm^{-1}$) bands, are usually assigned to the breathing mode of κ-point phonons of $A_{1g}$ symmetry and the $E_{2g}$ phonons of $sp^2$-carbon atoms, respectively.[38] It is well known that an increase in the D/G intensity ratio ($I_D/I_G$) indicates a lower degree of crystallinity in the graphite materials. In our case $I_D/I_G$ of the VC sample (1.2) is much larger than that of the catalyst with the graphene support (0.29). Therefore, the Raman results revealed that the as-prepared

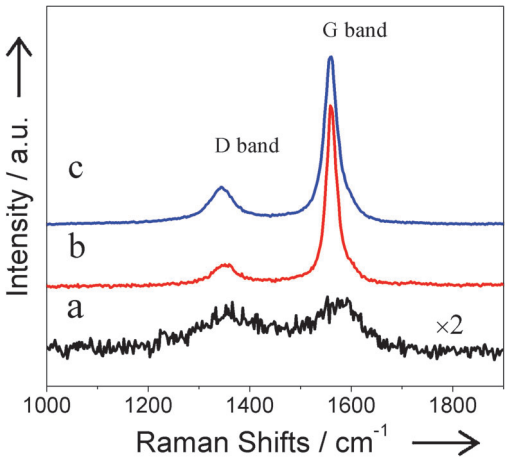


**Figure 2.** Raman spectra of a) 3.5 wt%Pt/VC, b) 3.5 wt%Pt/G, and c) 3.5 wt%Pt/G-r.

graphene catalyst has a higher degree of crystallinity than that with the VC support, in agreement with the XRD analysis.

Electron microscopy was used to characterize both the morphology of the carbon supports and the structural details of the Pt NPs (Figure 3). The supports of 3.5 wt%Pt/G and 3.5 wt%Pt/VC adopt preferential flake and sphere morphologies, respectively (SEM images in Figure 3a and b). On graphene, the Pt NPs are located mainly on the basal planes (Figure 3b). Pt particle size distributions were obtained from TEM images such as those shown in Figure 3c and e (for 3.5 wt%Pt/VC and 3.5 wt%Pt/G, respectively) and are reported in Figure 3i. Pt NPs of sizes of 3–6 and 2–5 nm were detected for 3.5 wt%Pt/G and 3.5wt%Pt/VC, respectively, and mean particle size values of around (4.4±1.0) and (3.9±0.9) nm were calculated for the two samples, close to the estimates from the XRD data (Table 1). The corresponding high-resolution transmission electron microscopy (HRTEM) images of 3.5wt%Pt/VC and 3.5wt%Pt/G (Figure 3d and f, respectively) display well-defined lattice fringes for the Pt NPs with lattice spacings of approximately 0.226–0.228 nm as expected for the (111) planes of Pt single-crystals. An additional insert is also provided in Figure 3f to display the well-defined lattice fringes of graphene, which in this case show a lattice spacing of 0.348 nm for the 002 planes of graphite. Sheet thicknesses of 6–18 layers were observed for 3.5 wt%Pt/G. TEM results for 2.0 wt%Pt/G and 5.0 wt%Pt/G also show mean Pt NP sizes of approximately 4.4 nm (Figure S1), which indicates that the Pt particle sizes are not affected by the Pt loading on the graphene support. XRD results from 2.0 wt%Pt/G and 5.0 wt%Pt/G are consistent with the TEM results (Figure S2 and Table S1).

The electronic structure of the Pt NPs was characterized by X-ray photoelectron spectroscopy (XPS). The Pt4f XPS spectra of 3.5 wt%Pt/VC and 3.5 wt%Pt/G are shown in Figure 4a and b, respectively, together with their deconvolution into three spin-split states obtained by fitting Gaussian peaks after Shirley-background subtraction. Three chemically different species were identified (Table 1), and the most intense pair of XPS peaks (at binding energies (BEs) of 71.4 and 74.7 eV for 3.5 wt%Pt/G, BE = 71.6 and 75.0 eV for 3.5 wt%Pt/VC) attributable to metallic $Pt^0$. The second Pt4f XPS doublet (BE = 72.6 and 75.9 eV for 3.5 wt%Pt/G, BE = 72.8 and 76.1 eV for 3.5 wt%Pt/VC) can be assigned to $Pt^{II}$, most likely from Pt in the form of PtO and/or $Pt(OH)_2$, and the third pair (BE = 74.9

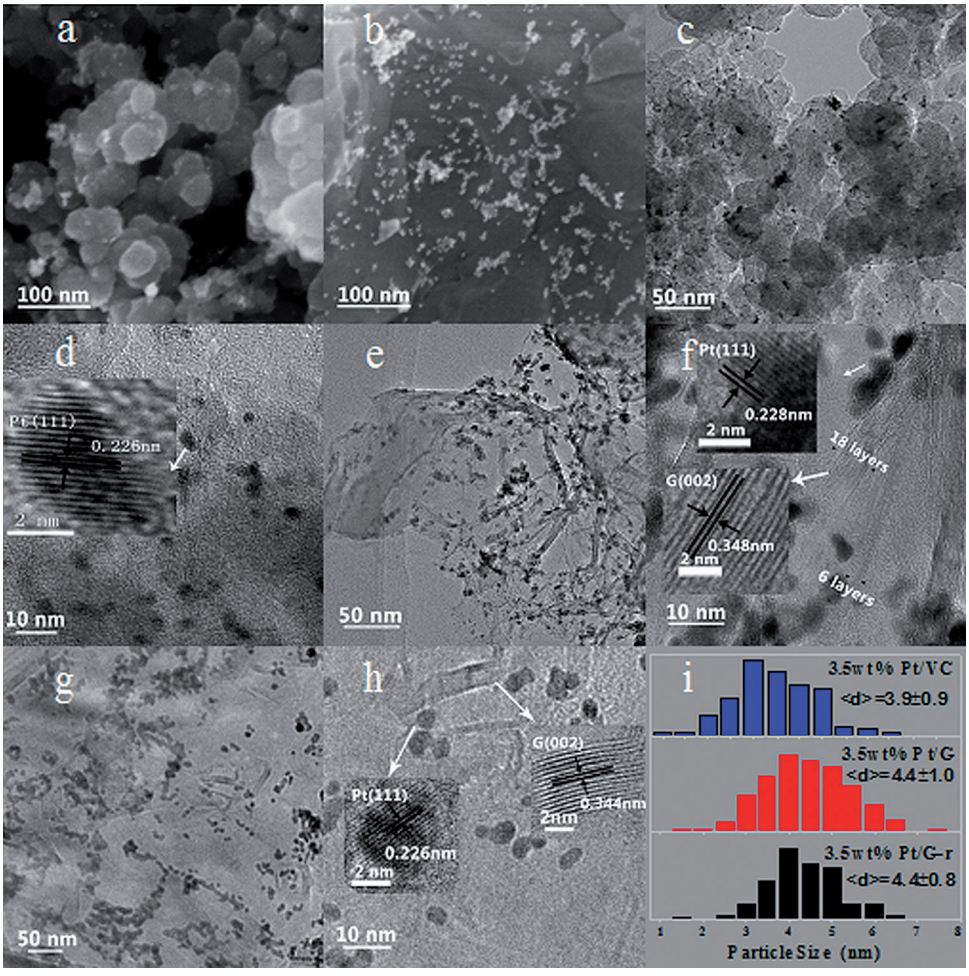


**Figure 3.** SEM images of a) 3.5 wt%Pt/VC and b) 3.5 wt%Pt/G. TEM images of c,d) 3.5 wt%Pt/VC, e,f) 3.5 wt%Pt/G, and g,h) 3.5 wt%Pt/G-r. i) Pt particle size distribution.

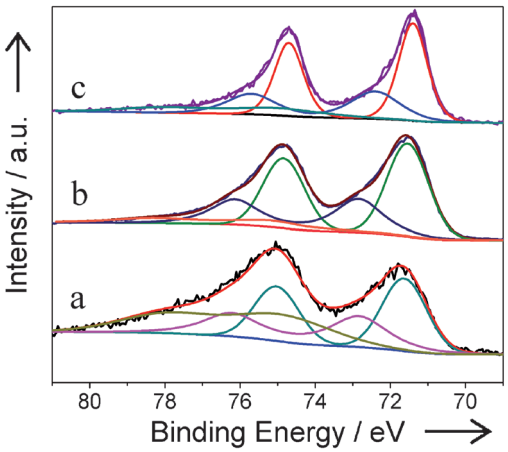


**Figure 4.** Pt 4f XPS spectra of a) 3.5 wt%Pt/VC, b) 3.5 wt%Pt/G, and c) 3.5 wt%Pt/G-r together with the spin-split peaks obtained by deconvolution.

and 78.0 eV for 3.5 wt%Pt/G, BE = 74.8 and 78.0 eV for 3.5 wt%Pt/VC) to $Pt^{IV}$, possibly $PtO_2$.[39–41] As a reference, the Pt 4f XPS peak positions of unsupported Pt and Pt dispersed on $SiO_2$ have been reported at BE = 71.0 and 71.1 eV, respectively.[42,43] In terms of quantitation of the composition of the Pt NPs, the fractions of the surface $Pt^0$, $Pt^{II}$, and $Pt^{IV}$ species on 3.5 wt%Pt/G and 3.5 wt%Pt/VC were estimated at 61/29/10% and 42/26/32%, respectively, although these values may underestimate the amount of metallic Pt, which may be located mostly in the core of the NPs and, therefore, their photoelectrons may be partially shielded by the oxidized outer shell. Interestingly, the amount of $Pt^0$ on the graphene-supported catalysts (61%) is higher than on the VC-supported catalysts (≈42%), and, in contrast, a much lower amount of $Pt^{IV}$ species is observed for 3.5 wt%Pt/G. XPS data for 2.0 wt%Pt/G and 5.0 wt%Pt/G yielded values of 58 and 59% for the amount of reduced Pt, respectively, the same (within experimental error) as that of 3.5 wt%Pt/G (Figure S3 and Table S1).

### Catalytic performance

The major products obtained from the hydrogenation of CAL with our catalysts were COL, HALD, and HALC, as expected. The main results from our kinetics studies are reported in Table 2. Comparable overall conversions were obtained with 3.5 wt%Pt/G and 3.5 wt%Pt/VC, approximately 20% less with 3.5 wt%Pt/G in the first 2 h of reaction, even though the surface area of 3.5 wt%Pt/G (57 $m^2 g^{-1}$) is much smaller than that of 3.5 wt%Pt/VC (198 $m^2 g^{-1}$). However, a significant difference was seen in selectivity: COL accounted for 82% of the products with 3.5 wt%Pt/G, but only approximately 27% with 3.5 wt%Pt/VC. A minor increase in the hydrogenation of the C=C bond to produce HALD was detected with the VC support, but the main difference was seen in the formation of other side products, which amounted to only a few percent of the converted CAL with 3.5 wt%Pt/G but more than half of the conversion with 3.5 wt%Pt/VC. These trends held for longer reaction times up to almost full conversion (Table 2). The selectivity of the graphene-based catalysts did not vary significantly as a function of Pt loading (Table S2).

**Table 2.** Kinetic results from CAL hydrogenation over Pt/G and Pt/VC catalysts.

| Catalyst | Conversion [%] | Selectivity [mol%] | | | |
|---|---|---|---|---|---|
| | | COL | HALD | HALC | Others[c] |
| 3.5 wt%Pt/G[a] | 73 | 82 | 8 | 6 | 4 |
| 3.5 wt%Pt/VC[a] | 89 | 27 | 10 | 5 | 58 |
| 3.5 wt%Pt/G[b] | 92 | 88 | 3 | 7 | 2 |
| 3.5 wt%Pt/VC[b] | 93 | 27 | 9 | 7 | 57 |

[a] Reaction conditions: 50 mg 3.5 wt%Pt/G, 1.00 g CAL, 30 mL isopropanol, 10 bar $H_2$, 333 K, 2 h. [b] Reaction conditions: 50 mg 3.5 wt%Pt/G, 1.00 g CAL, 30 mL isopropanol, 10 bar $H_2$, 333 K, 4 h. [c] Includes 1-(3-propoxyprop-1-enyl)benzene, cinnamyl formate, cinnamic acid, benzyl, cinnamate, 4,4-diphenylcyclohexa-1,5-dienyl acetate, and other condensation products that could be identified by GC–MS because of their large molecular weights.

More detailed kinetic runs for the CAL hydrogenation were performed with 3.5 wt%Pt/G to extract the appropriate kinetic parameters. The reaction rate was first order in CAL concentration (Figure 5a), consistent with results reported previously.[19,44] An Arrhenius analysis of the pseudo-first-order reaction constants calculated at three different temperatures yielded an apparent activation energy ($E_a$) of 18.8 kJ $mol^{-1}$ (Figure 5b). This value agreed with the findings of Oduro et al.,[44] who reported an $E_a$ of 17.3 kJ $mol^{-1}$ over unsupported PtCo nanocrystals.

The graphene catalysts were quite stable as shown by the data from recycling tests with 3.5 wt%Pt/G (Figure 6). After a second use of the catalyst, without any pretreatment in between, the activity of 3.5 wt%Pt/G was almost unchanged, and even after four cycles, the conversion of CAL declined only from 73 to 64%. In addition, the selectivity toward COL production increased slightly. Characterization by XRD (Figure 1c), Raman spectroscopy (Figure 2c), BET surface area measurements (Table 1), TEM (Figure 3c), and XPS (Figure 4c) all indicate minimal changes in the catalyst after four cycles: the Pt particles still remain well dispersed, with a mean size of approximately (4.4 ± 0.8) nm, and the composition of Pt surface states also stays unchanged compared to that of fresh 3.5 wt%Pt/G ($Pt^0$ = 59 vs. 61%, $Pt^{II}$ = 29 vs. 29%, $Pt^{IV}$ = 12 vs. 10%).

To test the role of the aromatic ring in the reaction selectivity with the graphene-based catalysts, a few additional kinetic runs were performed with crotonaldehyde (Table S3). Conversion rates comparable to those with CAL were observed, but the selectivity toward the unsaturated alcohol was lower in this case. Specifically, only 32% of the crotonaldehyde converted with 3.5 wt%Pt/G produced crotonalcohol. In addition, the kinetic hydrogenation reactions of furaldehyde, 3-(2-furyl)acrolein, and α-methylcinnamaldehyde were performed over 3.5 wt%Pt/G, respectively. High conversion was also observed with a high selectivity to the product for the hydrogenation of the C=O bond. The conversion of furaldehyde, 3-(2-furyl)acrolein, and α-methylcinnamaldehyde was 86, 92, and 89%, re-

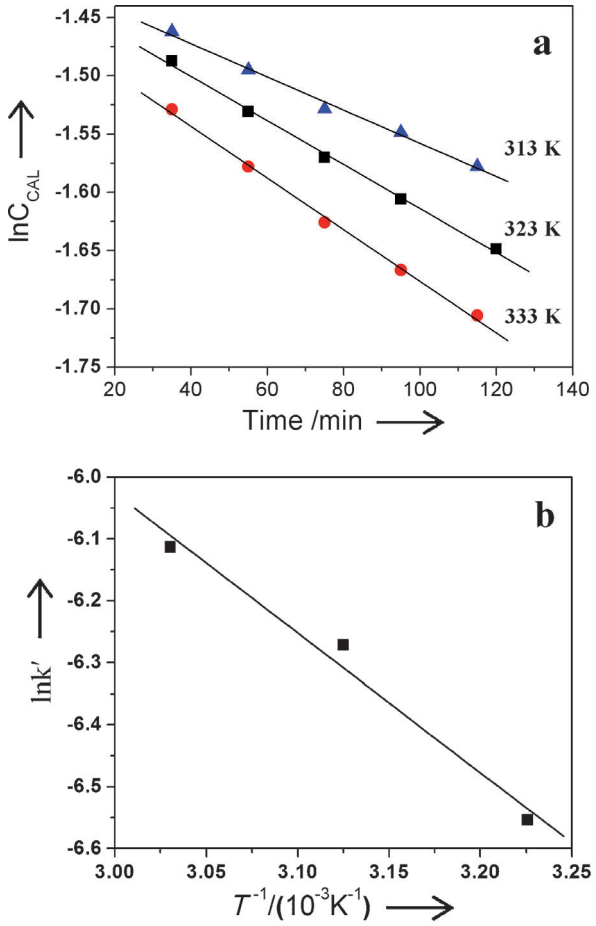


**Figure 5.** a) Plot of ln[CAL] versus reaction time for the conversion of CAL on 3.5 wt%Pt/G at three different temperatures. b) Arrhenius plot of the pseudo-first-order rate constants extracted from the data shown in (a). Reaction conditions: $P = 1.0$ MPa, stirring speed = 600 rpm, CAL = 1.0 g, catalyst = 3.5 wt%Pt/G (25 mg), isopropanol = 30 mL.

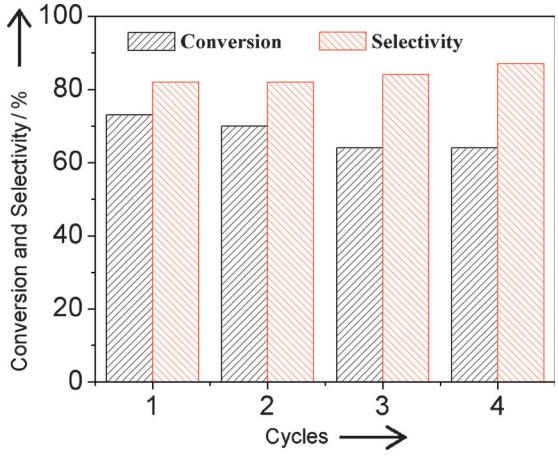


**Figure 6.** Stability test for 3.5 wt%Pt/G shown as performance versus number of recycling runs. Reaction conditions: 50 mg 3.5 wt%Pt/G, 1.00 g CAL, 30 mL isopropanol, 10 bar $H_2$, 333 K, 2 h.

spectively, which corresponds to 95, 82, and 71% of the selectivity for the hydrogenation of the C=O bond (Tables S4–S6). It would seem that the aromatic ring in CAL helps direct the hydrogenation of the C=O bond on the graphene-based catalysts.

### DFT calculations

The effect of the oxidation state of the Pt surface atoms on the catalytic activity and selectivity, suggested by the differences seen in the XPS data, was explored further by performing first-principles calculations. The adsorption energies of the C=O and C=C bonds of the CAL molecule on the top Pt atoms of three different Pt clusters (Pt6, Pt10, and Pt13) supported on a graphene sheet are shown in Figure 7, and the optimized

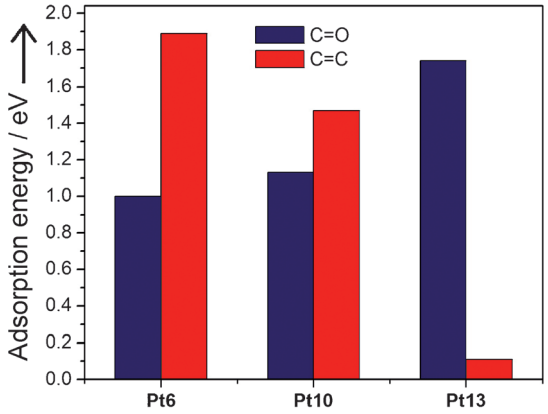


**Figure 7.** Calculated adsorption energies for CAL molecules bonded on Pt6, Pt10, and P13 clusters through their C=C (blue) and C=O (red) bonds.

structures of the CAL molecule adsorbed on the clusters, adsorbed through either the C=C or the C=O bond, are provided in Figure S4. Clearly, different trends are seen for the adsorption energies of CAL through the C=C and C=O bonds: they decreased gradually with increasing cluster size for adsorption through the C=C bond, but remain approximately constant if bonded through the C=O bond adsorption. Importantly, the relative stability of the C=C versus C=O bond adsorption modes flips with increasing cluster size: adsorption on small clusters is dominated by interaction with the C=C bond, which reverses with the Pt13 cluster. The implication is that larger clusters may favor the C=O-centered adsorption that leads to selectivity toward COL formation. This trend may be understood in terms of the electronic properties of the clusters, which may be extracted from the partial density of states (PDOS) of the supported Pt clusters on graphene (Figure 8). The most significant change seen with increasing cluster size is an increase in the metallic character of the valence band, which leads to an increase in the percentage of $Pt^0$ in the clusters.[30,45]

It can be concluded from these calculations that the adsorption energy of CAL through its C=C bond is much reduced with the increase in metallic character that comes with increasing Pt cluster size, and that adsorption through the C=O bond becomes favorable on larger Pt clusters. This hypothesis would need to be tested in the future with experiments that measure

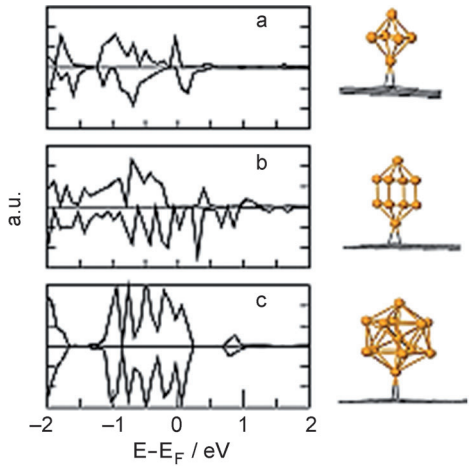


**Figure 8.** Calculated PDOS of the Pt 3d valence band for a) Pt6, b) Pt10, and c) Pt13 clusters. Right: respective optimized structures of the three Pt clusters on a graphene support. Color code: Yellow = Pt, gray = C.

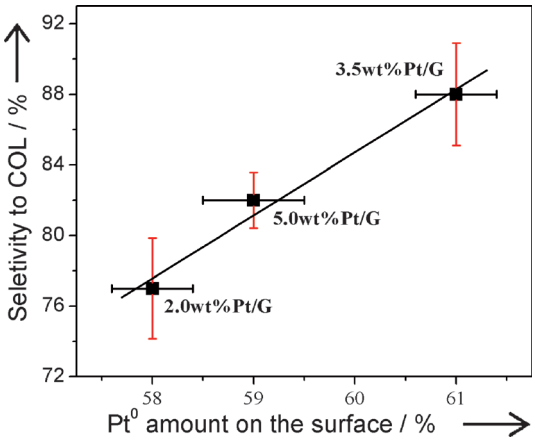


**Figure 9.** Selectivity toward COL production versus fraction of metallic Pt$^0$ atoms on the surface of *X* wt%Pt/G (*X* = 2.0, 3.5, and 5.0)

selectivity versus Pt particle size. Certainly, selectivity in CAL hydrogenation has already been shown to depend on particle size,[46–48] and it is reasonable to expect that the observed trends are the result of changes in the adsorption mode for the reactant, as suggested by our calculations. Moreover, on Pt(111) surfaces, both theoretical calculations[49–51] and surface-science experiments[52,53] have indicated a preference of the bonding of unsaturated aldehydes through their C=O bond, at least under certain circumstances.

## Discussion

In this report, we have provided characterization and catalytic data to indicate that Pt catalysts dispersed on graphene supports are much more selective for the hydrogenation of CAL to COL than equivalent catalysts made with other forms of carbon. A previous report with a similar Pt catalyst supported on reduced graphene oxide also described high selectivity toward the formation of the unsaturated alcohol,[35] but the authors ascribed their observations to the ability of graphene to enhance the dispersion of the metal, whereas our data indicate that this may not be a crucial factor. Indeed, according to the results from our characterization studies, similar mean particle size values were obtained for all the Pt/G catalysts (2.0 wt%Pt/G, 3.5 wt%Pt/G, and 5.0 wt%Pt/G) and 3.5 wt%Pt/VC synthesized here, but high selectivity was seen only with the graphene-based samples. Two other factors may account for the excellent selectivity to COL seen with the graphene-supported catalysts. First, there is the effect of the Pt electron structure. The XPS results indicate that the content of Pt$^0$ is higher on the surface of 3.5 wt%Pt/G (61%) than on 3.5 wt%Pt/VC (42%; Table 1). At the same time, the BE of the Pt 4f$_{7/2}$ peak for 3.5 wt%Pt/VC is higher, by approximately 0.3 eV, than that of 3.5 wt%Pt/G (BE = 71.7 vs. 71.4 eV). Interestingly, there seems to be a linear correlation between the amount of Pt$^0$ in the *X* wt%Pt/G catalysts and their selectivity toward COL production (Figure 9). These observations suggest that a zero-valent Pt surface is beneficial for the formation of unsaturated alcohols compared to a less reduced Pt surface. Also, it is clear that the amount of Pt$^0$ in the catalyst has a larger influence on the selectivity toward COL production than on the overall CAL conversion.[1] The DFT calculations suggest that this behavior may be related to the relative adsorption energies of C=C versus C=O bonds, which appears to shift toward the latter in larger and more metallic Pt clusters. Conversely, the oxidized Pt atoms may contribute to the conversion of CAL to other products. Specifically, the large fraction of Pt$^{IV}$ atoms seen on 3.5 wt%Pt/VC (32% versus 10% on 3.5 wt%Pt/G) may be responsible for the high-molecular-weight secondary products, which amount to more than half of the total conversion.

In addition to the effect of the electronic states of the Pt NPs, the special structure of the graphene support itself may also play an important role in the selectivity to COL.[20,54] The Raman spectroscopy results (Figure 2 and Table 1) indicate that the degree of crystallinity of the graphene support ($I_D/I_G = 0.29$) is higher than that of the VC support ($I_D/I_G = 1.2$), which means that the size of the graphene electronic network around a given Pt NP is bigger than that of the VC support. Aromatic rings can be adsorbed easily on the surface of graphene through intermolecular $\pi$–$\pi$ interactions.[31] Therefore, the graphene basal planes may interact with the benzene ring and affect the adsorption of the CAL molecule through the terminal C=O bond. This synergy may lead to the observed higher selectivity toward COL production. This hypothesis is supported by the lower selectivity seen in the hydrogenation experiments with crotonaldehyde using the same graphene-based catalysts. It can be argued that the absence of an aromatic moiety in this case prevents the molecule from adopting a preferential adsorption geometry on the graphene support, and that its hydrogenation is controlled mainly by the interaction with the metal. In contrast, the bonding of the benzene ring in CAL with the graphene may provide an additional constraint on the access of the C=C bond to the Pt surface, which minimizes the extent of its hydrogenation. The hydrogenation experiments of 3-(2-furyl)acrolein and $\alpha$-methylcinnamaldehyde, which have $\pi$ bonds, also confirm this hypothesis.

## Conclusions

Graphene-supported Pt catalysts (Pt/G) have been prepared and exhibit excellent catalytic performances in terms of selectivity for the hydrogenation of unsaturated aldehydes. Specifically, high selectivity was observed for cinnamal alcohol (88%) production from cinnamaldehyde, much higher than that achieved with Pt catalysts dispersed on other forms of carbon. This special catalytic performance has been attributed to a strong electronic interaction between the Pt nanoparticles and the graphene, which leads to the creation of a much larger fraction of metallic $Pt^0$ surface sites. Indeed, the experimental results suggest that the larger the fraction of $Pt^0$ sites on the surface of the Pt/G catalyst, the higher its selectivity toward cinnamal alcohol production. Also, DFT calculations indicated that cinnamaldehyde adsorption through its C=O bond becomes more favorable with the increasing metallic character of the Pt clusters. In addition, the special electronic structure of the graphene support itself, which favors intermolecular $\pi$–$\pi$ interactions with aromatic molecules such as cinnamaldehyde, is also likely to play an important role in the selectivity toward cinnamal alcohol.

## Experimental Section

### Catalyst preparation

The graphene support was prepared by an in situ self-generating template route described previously.[36] Briefly, polyacrylic weak-acid cation-exchanged resin (PWAC) was added to aqueous $FeCl_2{\cdot}7H_2O$, the solution was stirred for 10 h under $N_2$, and the solid was separated by centrifugation. This process was repeated four times. The solid was collected after two washing/centrifugation cycles and dried under vacuum. The solid was then carbonized at 1100 °C for 0.5 h under $N_2$. To remove the Fe species thoroughly, the sample was treated in 10% HCl at 90 °C for 8 h. The solids were separated by several additional washing/centrifugation cycles, and then dried in a vacuum oven at 80 °C for 6 h. The graphene sample is denoted as G.

The 3.5 wt%Pt/graphene catalyst was prepared according to a procedure described earlier.[36] Typically, graphene (0.50 g) was suspended in deionized water (50 mL) and ultrasonicated for 0.5 h to form a dispersed slurry. A solution of $H_2PtCl_6{\cdot}6H_2O$ (4.65 g, 19.31 mmol $L^{-1}$) was added to the slurry, and the concentration of Pt precursor was kept at $\approx$2 mmol $L^{-1}$. The slurry was ultrasonicated for 0.5 h and then placed in an ice bath with vigorous stirring for another 0.5 h. The temperature of the ice bath was kept at 2–4 °C, and the pH was adjusted to 8.0 by using NaOH solution (0.1 mol $L^{-1}$). Afterwards, an excess of $NaBH_4$ (0.4 mol $L^{-1}$) was added to the mixture, which was mixed vigorously in the ice bath using high-speed stirring for 3 h and kept in the ice bath for another 10 h. Finally, 3.5 wt%Pt/G was obtained after filtration, washing with deionized water until no chloride was detected, washing with ethanol, and drying at 60 °C for 10 h. The 2.0 wt%Pt/G, 5.0 wt%Pt/G, and 3.5 wt%Pt/VC catalysts were prepared by following the same method.

### Catalyst characterization

XRD analysis of the catalysts was performed by using a Rigaku D/max-IIIB diffractometer with a $CuK_\alpha$ ($\lambda = 1.5406$ Å) radiation source set at a total power of 40 kV and 20 mA. Raman spectra were recorded by using a Jobin Yvon HR 800 micro-Raman spectrometer and $a = 457.9$ nm excitation source. The laser beam was focused on the sample with a 50× objective. XPS studies were performed by using a Kratos-AXIS ULTRA DLD with an $AlK_\alpha$ radiation source. Conventional TEM experiments were performed by using a JOEL model JEM-210 electron microscope working with an acceleration voltage of 200 kV. SEM images were acquired by using a Hitachi S-4800 field-emission electron microscope at 20 kV. The surface areas were derived from $N_2$ sorption measurements at 77 K by using a Micromeritics Tristar 3000 physisorption instrument. In each case, the sample was degassed under vacuum at 423 K for 4 h before the measurements.

### Reaction procedure

The activity of all catalysts was measured in a 100 mL stirred autoclave. The catalyst (50 mg) was immersed in isopropanol (15 mL; analytical reagent grade). After removing traces of dissolved $O_2$ by flushing three times with $N_2$ at 5 bar and three times with $H_2$ at 5 bar, 10 bar of $H_2$ was added, and the temperature was increased to 383 K. The catalyst was kept under those conditions for 1 h for activation. A mixture of CAL (1.00 g) and isopropanol (15 mL) was then added to the autoclave. After flushing again three times with $N_2$ at 5 bar and three times with $H_2$ at 5 bar, the reaction was allowed to proceed at 333 K under 10 bar of $H_2$. The hydrogenation reactions of crotonaldehyde, furaldehyde, $\alpha$-methylcinnamaldehyde, and 3-(2-furyl)acrolein were the same as above. Detailed reaction conditions are given in each table foot. The products were analyzed by GC (Agilent 7820 A) with flame ionization detection (FID) and an HP-5 capillary column (30 m × 0.32 mm × 0.25 μm). The products were further identified by GC–MS (Agilent 6890/5973N).

### DFT computations

The calculations reported here were performed by using periodic, spin-polarized DFT as implemented in the Vienna ab initio program package (VASP).[55,56] The electron–ion interactions were described by using the projector augmented wave (PAW) method proposed by Blöchl[57] and implemented by Kresse.[58] The PBE functional[59] was used as the exchange-correlation functional approximation and a plane wave basis set with an energy cutoff of 400 eV was employed. Only the gamma point was used in the brillouin zone sampling. All atoms were allowed to relax during the structure optimization, and no symmetry was imposed. The optimization was stopped when the maximum force on the atoms was smaller than 0.05 eV $Å^{-1}$. A 7×7 cell was used for graphene in the calculations, amounting to 98 carbon atoms. The distance between neighboring cells was 12 Å. Three different Pt clusters supported on the graphene were studied, with 6 (Pt6), 10 (Pt10), and 13 (Pt13) Pt atoms. The adsorption energy of CAL was calculated as [Eq. (1)]:

$$\text{Adsorption energy} = E_{CAL} + E_{Pt/G} - E_{CAL/Pt/G} \quad (1)$$

in which $E_{CAL}$, $E_{Pt/G}$, and $E_{CAL/Pt/G}$ are the total energy of the CAL molecule, the Pt clusters supported on the graphene, and the adsorbed CAL on the supported Pt clusters, respectively.

## Acknowledgements

*This work is supported by the Program for New Century Excellent Talents in Heilongjiang Provincial University (1155-NCET-014), the Natural Science Foundation of Heilongjiang Province (B200805), the Foundation of Educational Commission of Heilongjiang Province of China (11531286), the Postdoctoral Science-research Developmental Foundation of Heilongjiang Province of China (LBH-Q12022), the Innovative Research Team in Heilongjiang University (Hdtd2010-10), the Program for Innovative Research Team in University (IRT-1237), the Technology Foundation for Selected Overseas Chinese Scholar, and the Ministry of HRSS of China and the U. S. National Science Foundation. B.L. is supported by a SYNL-T.S. K Research Fellowship. B.L. is grateful for a financial grant from the Institute of Metal Research (Y3NBA211A1). The computing resource is partly supported by the ShenYang Branch, Supercomputing Center of CAS.*

**Keywords:** graphene · heterogeneous catalysis · hydrogenation · platinum · supported catalysts

[1] P. Gallezot, D. Richard, *Catal. Rev. Sci. Eng.* **1998**, *40*, 81 – 126.
[2] P. Claus, *Top. Catal.* **1998**, *5*, 51 – 62.
[3] U. K. Singh, M. A. Vannice, *Appl. Catal. A* **2001**, *213*, 1 – 24.
[4] X. X. Han, R. X. Zhou, B. H. Yue, X. M. Zheng, *Catal. Lett.* **2006**, *109*, 157 – 161.
[5] Y. Li, C. H. Ge, J. Zhao, R. X. Zhou, *Catal. Lett.* **2008**, *126*, 280 – 285.
[6] P. Mäki-Arvela, J. Hájek, T. Salmi, D. Y. Murzin, *Appl. Catal. A* **2005**, *292*, 1 – 49.
[7] J. March, *Advanced Organic Chemistry, 2nd ed.*, McGraw-Hill Kogakusha, Tokyo, **1977**.
[8] Y. J. Zhu, F. Zaera, *Catal. Sci. Technol.* **2014**, *4*, 955 – 962.
[9] G. R. Bertolini, C. I. Cabello, M. Muñoz, M. Casella, D. Gazzoli, I. Pettiti, G. Ferraris, *J. Mol. Catal. A* **2013**, *366*, 109 – 115.
[10] T. Mitsudome, K. Kaneda, *Green Chem.* **2013**, *15*, 2636 – 2654.
[11] H. Vu, F. Gonçalves, R. Philippe, E. Lamouroux, M. Corrias, Y. Kihn, D. Plee, P. Kalck, P. Serp, *J. Catal.* **2006**, *240*, 18 – 22.
[12] Z. Guo, C. Xiao, R. V. Maligal-Ganesh, L. Zhou, T. W. Goh, X. Li, D. Tesfagaber, A. Thiel, W. Huang, *ACS Catal.* **2014**, *4*, 1340 – 1348.
[13] G. Cordier, Y. Colleuille, P. Fouilloux in *Catalyse par les Métaux* (Eds.: B. Imelik, G. A. Martin, A. J. Renouprez), Editions du CNRS, Paris, **1984**, p. 349.
[14] G. Cordier (S. A. Rhone-Poulenc, France) F2,329, 628, **1975**; [*Chem. Abstr.* **1977**, *87*, 38862s].
[15] S. Bhogeswararao, D. Srinivas, *J. Catal.* **2012**, *285*, 31 – 40.
[16] H. G. Manyar, B. Yang, H. Daly, H. Moor, S. McMonagle, Y. Tao, G. D. Yadav, A. Goguet, P. Hu, C. Hardacre, *ChemCatChem* **2013**, *5*, 506 – 512.
[17] K. Liberková, R. Touroude, *J. Mol. Catal. A* **2002**, *180*, 221 – 230.
[18] A. Huidobro, A. Sepúlveda-Escribano, F. Rodríguez-Reinoso, *J. Catal.* **2002**, *212*, 94 – 103.
[19] E. V. Ramos-Fernández, A. F. P. Ferreira, K. A. F. Sepúlveda-Escribano, F. Rodríguez-Reinoso, *J. Catal.* **2008**, *258*, 52 – 60.
[20] S. Handjani, E. Marceau, J. Blanchard, J. M. Krafft, M. Che, P. Mäki-Arvelad, N. Kumard, J. Wärnåd, D. Y. Murzind, *J. Catal.* **2011**, *282*, 228 – 236.
[21] Z. Guo, Y. T. Chen, L. S. Li, X. M. Wang, G. L. Hallerb, Y. H. Yang, *J. Catal.* **2010**, *276*, 314 – 326.
[22] D. S. Su, J. Zhang, B. Frank, A. Thomas, X. Wang, J. Paraknowwitsch, R. Schlögl, *ChemSusChem* **2010**, *3*, 169 – 180.
[23] J. Zhang, X. Liu, R. Blume, A. Zhang, R. Schlögl, D. S. Su, *Science* **2008**, *322*, 73 – 77.
[24] D. S. Su, R. Schlögl, *ChemSusChem* **2010**, *3*, 136 – 168.
[25] R. Wang, J. Yang, K. Shi, B. Wang, L. Wang, G. Tian, B. Bateer, C. Tian, P. Shen, H. Fu, *RSC Adv.* **2013**, *3*, 4771 – 4777.
[26] J. Yang, C. Tian, L. Wang, H. Fu, *Mater. Chem.* **2011**, *21*, 3384 – 3390.
[27] K. S. Novoselov, A. K. Geim, S. V. Morozov, D. Jiang, Y. Zhang, S. V. Dubonos, I. V. Grigorieva, A. A. Firsov, *Science* **2004**, *306*, 666 – 669.
[28] M. D. Stoller, S. J. Park, Y. W. Zhu, J. H. An, R. S. Ruoff, *Nano Lett.* **2008**, *8*, 3498 – 3502.
[29] D. Q. Yang, G. X. Zhang, E. Sacher, M. José-Yacamán, N. Elizondo, *J. Phys. Chem. B* **2006**, *110*, 8348 – 8356.
[30] G. Ramos-Sanchez, P. B. Balbuena, *Phys. Chem. Chem. Phys.* **2013**, *15*, 11950 – 11959.
[31] J. H. Yang, G. Sun, Y. J. Gao, H. B. Zhao, P. Tang, J. Tan, A. H. Lu, D. Ma, *Energy Environ. Sci.* **2013**, *6*, 793 – 798.
[32] Z. Zhang, H. Huang, X. Yang, L. Zang, *J. Phys. Chem. Lett.* **2011**, *2*, 2897 – 2905.
[33] J. Li, C. Liu, Y. J. Liu, *Mater. Chem.* **2012**, *22*, 8426 – 8430.
[34] Z. Sun, Z. Rong, Y. Wang, Y. Xia, W. Du, Y. Wang, *RSC Adv.* **2014**, *4*, 1874 – 1878.
[35] J. J. Shi, R. F. Nie, P. Chen, Z. Y. Hou, *Catal. Commun.* **2013**, *41*, 101 – 105.
[36] L. Wang, C. G. Tian, H. Wang, Y. G. Ma, B. L. Wang, H. G. Fu, *J. Phys. Chem. C* **2010**, *114*, 8727 – 8733.
[37] Z. T. Liu, C. X. Wang, Z. W. Liu, J. Lu, *Appl. Catal. A* **2008**, *344*, 114 – 123.
[38] F. Tuinstra, J. L. Koenig, *J. Chem. Phys.* **1970**, *53*, 1126 – 1130.
[39] X. M. Feng, R. M. Li, C. H. Hu, W. H. Hou, *J. Electroanal. Chem.* **2011**, *657*, 28 – 33.
[40] S. Sharma, A. Ganguly, P. Papakonstantinou, X. M. P. Miao, M. X. Li, J. L. Hutchison, M. Delichatsios, S. J. Ukleja, *J. Phys. Chem. C* **2010**, *114*, 19459 – 19466.
[41] X. W. Yu, S. Y. Ye, *J. Power Sources* **2007**, *172*, 145 – 154.
[42] Z. Zhu, F. Tao, F. Zheng, R. Chang, Y. M. Li, L. Heinke, Z. Liu, M. Salmeron, G. A. Somorjai, *Nano Lett.* **2012**, *12*, 1491 – 1497.
[43] F. Y. Zhao, Y. Ikushima, M. Shirai, T. Ebina, M. Arai, *J. Mol. Catal. A* **2002**, *180*, 259 – 265.
[44] W. O. Oduro, N. Cailuo, K. M. K. Yu, H. W. Yang, S. C. Tsang, *Phys. Chem. Chem. Phys.* **2011**, *13*, 2590 – 2602.
[45] B. S. Mun, M. Watanabe, M. Rossi, V. Stamenkovic, N. M. Markovic, P. N. J. Ross, *J. Chem. Phys.* **2005**, *123*, 204717.
[46] A. J. Plomp, H. Vuori, A. Krause, I. Outi, K. P. de Jong, J. H. Bitter, *Appl. Catal. A* **2008**, *351*, 9 – 15.
[47] A. K. Prashar, S. Mayadevi, D. R. Nandini, *Catal. Commun.* **2012**, *28*, 42 – 46.
[48] Y. Yuan, S. Yao, M. Wang, S. Lou, N. Yan, *Curr. Org. Chem.* **2013**, *17*, 400 – 413.
[49] F. Delbecq, P. Sautet, *J. Catal.* **2002**, *211*, 398 – 406.
[50] D. Loffreda, F. Delbecq, F. Vigne, P. Sautet, *Angew. Chem. Int. Ed.* **2005**, *44*, 5279 – 5282; *Angew. Chem.* **2005**, *117*, 5413 – 5416.
[51] D. Loffreda, F. Delbecq, F. Vigne, P. Sautet, *J. Am. Chem. Soc.* **2006**, *128*, 1316 – 1323.
[52] J. C. de Jesús, F. Zaera, *J. Mol. Catal. A* **1999**, *138*, 237 – 240.
[53] J. C. de Jesús, F. Zaera, *Surf. Sci.* **1999**, *430*, 99 – 115.
[54] G. Szöllösi, B. Török, L. Baranyi, M. Bartók, *J. Catal.* **1998**, *179*, 619 – 623.
[55] G. Kresse, J. Furthmüller, *Comput. Mater. Sci.* **1996**, *6*, 15 – 50.
[56] G. Kresse, J. Furthmüller, *Phys. Rev. B* **1996**, *54*, 11169 – 11186.
[57] P. E. Blöchl, *Phys. Rev. B* **1994**, *50*, 17953 – 17979.
[58] G. Kresse, D. Joubert, *Phys. Rev. B* **1999**, *59*, 1758 – 1775.
[59] J. P. Perdew, K. Burke, M. Ernzerhof, *Phys. Rev. Lett.* **1996**, *77*, 3865 – 3868.

Received: July 23, 2014
Revised: August 6, 2014
Published online on October 1, 2014